Endothelialized microvessels fabricated by microfluidics facilitate osteogenic differentiation and promote bone repair

Jiayuan Wang[a,#], Huan Wang[a,#], Yong Wang [b,#], Zhao Liu[a], Zexi Li[a], Jiaying Li[a], Qixin Chen[a], Qingchen Meng[a], Wenmiao Will Shu[c], Junxi Wu[c], Can Xiao[a,*], Fengxuan Han[a,*], Bin Li[a,d,e,*]

[a] College of Chemistry, Chemical Engineering and Materials Science, Orthopaedic Institute, Departments of Orthopaedic Surgery and Stomatology, The First Affiliated Hospital, Suzhou Medical College, Soochow University, Suzhou, Jiangsu 215007, China;

[b] Department of Orthopedic Surgery, The Affiliated Yixing Hospital of Jiangsu University, Wuxi, Jiangsu 214200, China;

[c] Department of Biomedical Engineering, University of Strathclyde, Glasgow, G1 1QE, UK;

[d] The Affiliated Haian Hospital of Nantong University, Haian, Nantong 226600, Jiangsu, China.

[e] Collaborative Innovation Center of Hematology, Soochow University, Suzhou, Jiangsu 215000, China.

[#] These authors equally contributed to this study.

* Corresponding to:

Prof. Bin Li, Rm 201 Bldg Jiwu, Soochow University (North Campus), 178 Ganjiang Rd, Suzhou, Jiangsu 215007, China

Tel. & Fax: (+86) 512-6778-1163

E-mails: binli@suda.edu.cn (BL); fxhan@suda.edu.cn (FH); canxiao0511@163.com (CX).

Abstract

In bone tissue engineering, vascularization is one of the critical factors that limit the effect of biomaterials for bone repair. While various approaches have been tried to build vascular networks in bone grafts, lack of endothelialization still constitutes a major technical hurdle. In this study, we have developed a facile technique to fabricate endothelialized biomimetic microvessels (BMVs) from alginate-collagen composite hydrogels within a single step using microfluidic technology. BMVs with different sizes could be readily prepared by adjusting the flow rate of microfluids. All BMVs supported perfusion and outward penetration of substances in the tube. Endothelial cells could adhere and proliferate on the inner wall of tubes. It was also found that the expression of CD31 and secretion of BMP-2 and PDGF-BB were higher in the rat umbilical vein endothelial cells (RUVECs) in BMVs than those cultured on hydrogel. When co-cultured with bone marrow mesenchymal stem cells (BMSCs), endothelialized BMVs promoted the osteogenic differentiation of BMSCs compared to those in acellular BMV group. *In vivo*, markedly enhanced new bone formation was achieved by endothelialized BMVs in a rat critical-sized calvarial defect model compared to those with non-endothelialized BMVs or without BMVs. Together, findings from both *in vitro* and *in vivo* studies have proven that endothelialized BMVs function to facilitate osteogenesis and promote bone regeneration, and therefore might present an effective strategy in bone tissue engineering.

Keywords: Endothelialized biomimetic microvessels; alginate-collagen hydrogel; microfluidics; GelMA; bone repair

1. Introduction

As a highly vascularized tissue, bone contains a skeletal vascular network which plays a critical role in its development, regeneration and remodeling [1, 2]. The blood vessels in bone not only function to deliver oxygen, nutrients, hormones, growth factors and other neurotransmitters secreted by tissues (such as brain-derived serotonin) to bone to maintain the survival of bone cells and stimulate their activities, but also clear the metabolites from bone tissue to maintain its homeostasis [3-5]. Numerous studies have also shown that neovascularization plays an important role in bone repair and regeneration [6, 7]. For example, insufficient vascularization resulted in failure of bone repair [8], yet rebuilding blood vessels facilitated bone repair [9, 10]. In addition, the endothelial cells (ECs) which form the innermost layer of blood vessel walls have important signaling functions that regulate the growth, patterning, homeostasis and regeneration of surrounding organs/tissues. In the skeletal system, blood vessels regulate development, regenerative bone formation and hematopoietic function by providing vascular niches for cells [11].

At present, pedicled vascularized bone grafts are considered the gold standard in clinical practice for reconstruction of bone defects due to their predictable pedicled blood vessels and good bone-forming ability. For example, vascularized fibular grafts increased the vascularity of traumatized region and helped eliminate infection at the injury site [12]. Recently, microvessels extracted from autologous tissue have been used to facilitate cardiomyocyte engraftment following myocardial injury [13], suggesting the potential of using microvessels for tissue regeneration. However, the challenges associated with autologous blood vessel harvesting, including limited supply area, surgical wounds and pain to patients, largely hinder the application of autologous blood vessels-containing tissue grafts for bone repair.

To overcome such limitation, tissue engineering has been used as an alternative approach for bone repair [14]. Different cells, growth factors or their combination with scaffold materials have been proven to promote bone healing. A randomized control study indicated that patients with open tibial fracture treated with collagen sponges

loaded with recombinant human bone morphogenetic proteins (rhBMP-2) had significantly better fracture healing compared to non-treated patients [15]. In a clinical trial, autologous BMSCs mixed with fibrin were locally injected into the long bone fractures of the patients, and significant fracture healing acceleration was observed [16]. A variety of biomaterials have also been developed for repairing bone defect [17, 18]. As angiogenesis and osteogenesis are tightly coupled during bone development and regeneration, vascularization of biomaterials remains a major challenge at the early stage of bone repair process. To address this problem, various pro-vascularization approaches, such as applying growth factors and ECs, have been developed [19-22]. Incorporation of exogenous vascular endothelial growth factor (VEGF) in bone scaffolds, for example, markedly promoted new blood vessel formation and bone regeneration [23, 24]. Other bioactive factors, such as osteoprotegerin, have also been reported to enhance the recruitment of endothelial progenitor cells and angiogenesis at the bone defect site, and improve the survival rate of artificial bone grafts [25]. However, the success of this strategy relies on rapid formation of microvascular network and establishment of effective perfusion in the bone graft, which are significantly influenced by the health condition of recipient and the location of implant. Alternatively, ECs regulates tissue morphogenesis by secreting growth factors and cytokines and expressing signaling molecules on the cell surface. ECs can secrete BMPs, VEGF and other growth factors to stimulate cell proliferation and differentiation and further promote bone development and regeneration [26-28]. Incorporating vascular ECs, therefore, provides another way to promote vascularization [29].

Further, tissue engineered biomimetic microvessels (BMVs), instead of discrete vascular cells, have emerged as an alternate solution to accelerate vascularization. In addition, the richer the blood vessels are, the more conducive to the nutrient supply of tissues, and the thinner the blood vessel wall, the more conducive to the realization of substance exchange between blood vessels and tissues [10]. BMVs, commonly formed by encapsulating or seeding blood vessel cells in a prefabricated tube composed of hydrogel, may function to deliver oxygen and nutrients as well as metabolic waste, and

as a result, promote cell proliferation and other physiological activities. In addition, the exchange of growth factors could also be achieved by BMVs [30, 31]. To date, a number of engineering technologies such as micro-modeling [32], coaxial electrospinning [33], 3D printing [34-36] and microfluidic technology [37-39] have been used for building BMVs *in vitro* [40-42]. Among them, microfluidic technology (or microfluidics), possessing unique advantages including low cost, simple operation and flexibility in controlling microscale fluid, has been widely used in the preparation of microscale constructs [43-45]. Importantly, microfluidic technology allows facile fabrication of hollow microfibers of different sizes by simply varying the flow rate of fluids without the need to use any complex equipment [46-48]. Various cells, including human umbilical vein endothelial cells (HUVECs), could directly adhere and proliferate on the inner wall of hollow fibers [49-51].

In this study, we aimed to load ECs in the lumen of BMVs to prepare endothelialized BMVs and explore the potential for facilitating osteogenic differentiation *in vitro* and promoting bone regeneration *in vivo* (Scheme 1). Instead of using conventional two-step approach to prepare cell-loaded BMVs, i.e., fabricating acellular BMVs followed by culturing cells within them, we developed a facile microfluidics-based approach which allowed formation of endothelialized BMVs within a single step. BMVs with different lumen sizes made from alginate-collagen composite hydrogels were fabricated by adjusting the flow rate of the inner and outer phases in a coaxial needle. The growth of rat umbilical vein endothelial cells (RUVECs) in the BMVs, their secretion of growth factors including BMP-2 and PDGF-BB, and the expression of EC marker CD31 was analyzed. The effect of RUVECs-loaded BMVs (RUVEC-BMVs) on the osteogenic differentiation of rat bone marrow mesenchymal stem cells (rBMSCs) was determined *in vitro*. To study the bone repair effect of RUVEC-BMVs *in vivo*, RUVEC-BMVs were implanted in a rat critical-sized calvarial defect model and encapsulated with GelMA. Out findings demonstrate that endothelialized BMVs markedly facilitated osteogenesis and promoted bone

regeneration. Therefore, this study might provide a facile yet effective strategy for bone tissue engineering.

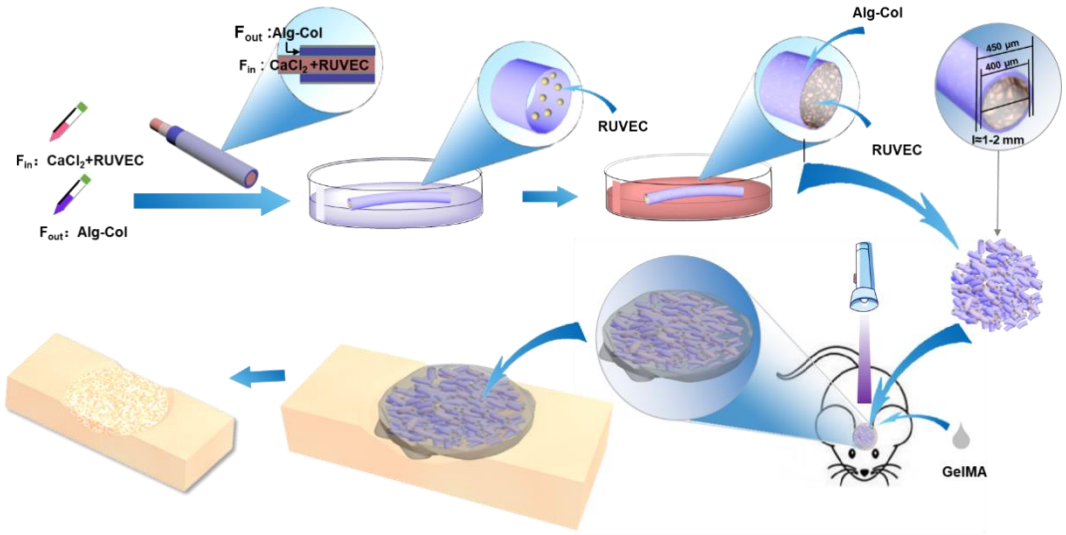

Scheme 1. Schematic illustration of the fabrication and application of BMVs loaded with RUVECs. The coaxial needle is divided into internal and external phases. The inner phase is calcium chloride containing cells and the outer phase is sodium alginate mixed with collagen. The two phases are quickly crosslinked upon contact, resulting in formation of RUVEC-BMVs. After the RUVEC-BMVs are implanted into a critical-sized calvarial defect of rat, GelMA solution is applied and then cured upon blue light irradiation to form a gel to cover the defect.

2. Materials and methods

2.1. Materials

Sodium-alginate powder (Alg, 80-120 cP) was purchased from Wak Pure Chemical Industries (Osaka, Japan). Calcium chloride ($CaCl_2$) was purchased from Sinopharm Chemical Regent Co., Ltd (Shanghai, China). Collagen (Col, Cellmatrix Type I-A) was purchased from Nitta Gelatin Inc. (Japan). Fluorescein isothiocyanate-labeled bovine serum albumin (FITC-BSA) was purchased from Solarbio Life Sciences (Beijing, China). Fluorescence microspheres were purchased from Aladdin Industrial Corporation (Shanghai, China). All chemicals were used without further purification.

RUVECs were purchased from Huato Biotechnology Co., Ltd (Guangzhou, China). Alpha's modified Eagle's medium (α-MEM) was purchased from Hyclone (UT, USA).

2.2. Preparation of Alginate-collagen (Alg-Col) Hydrogels

Sodium-alginate powder was dissolved in deionized water to obtain Alg solution (20 mg/mL, wt/v). The Alg hydrogels were fabricated by adding Alg solution into the 12-well plate and then adding $CaCl_2$ solution (30 mg/mL, wt/v). Collagen (Col) membrane was prepared by adding Collagen solution (3 mg/mL, wt/v) into 12-well culture plate and then adjusting pH to neutral. The Alg-Col mixed solution was prepared, in which the concentration of collagen and alginate was 2 mg/mL and 20 mg/mL, respectively. The Alg-Col hydrogels were fabricated by adding the Alg-Col solution into the 12-well plate, then adding $CaCl_2$ solution and Alg was rapidly crosslinked to obtain hydrogel. The prepared hydrogel was placed in the oven at 37 ℃ for 15 minutes to remove water from the surface. Then the water contact angle was measured by droplet method using a contact angle analyzer (JGW360B, China). Three samples were used in the water contact angle test. For mechanical testing, the Alg-Col solution was used to prepare hydrogel cylinders with a diameter of 9 mm and a height of 6 mm. The hydrogel cylinders were subjected to a compression test using a mechanical testing machine (HY-0580, Shanghai Heng Wing Precision Instrument Co., Ltd., Shanghai, China) at a speed of 1 mm/min. The compressive strength was defined as the stress at 60% deformation in a stress-strain curve, wherein the slope of 0-20% deformation was recorded as the compressive modulus. Five samples were used in the mechanical test.

2.3. Preparation of Alg-Col BMVs

The process of fabricating BMVs using microfluidic technology in one step is shown in Scheme 1. Using a coaxial needle, BMVs with different sizes were easily obtained by changing the flow rate of internal and external phases. The Alg-Col solution (Alg, 20 mg/mL; Col, 2 mg/mL) was used as the outer phase fluid and $CaCl_2$ solution (30 mg/mL) as the inner phase fluid. The flow rate of fluid in inner and outer phase

could be controlled by the syringe pump. When the two phases contact, sodium alginate reacted with Ca^{2+} and crosslinking happened rapidly. As a result, the Alg hollow fibers were obtained. Then these fibers were placed in petri dishes containing $CaCl_2$ solution for further cross-linking. Using coaxial needles, hollow fibers with different sizes could be easily obtained by changing the velocity of the inner and outer phases. The inner diameter of hollow fiber increases with the decrease of inner flow velocity when the outer flow velocity remains unchanged. When the flow rate of outer phase was 0.1 mL/min and the flow rate of inner phase was 0.3 mL/min, the BMV wall thickness was 100±20 μm. When the flow rate of outer phase was maintained at 0.1 mL/min and the flow rate of inner phase was reduced to 0.1 mL/min, the BMV wall thickness increased to 150±20 μm. In addition, when the flow rate of outer phase was maintained at 0.1 mL/min and the flow rate of inner phase further decreased to 0.05 mL/min, the wall thickness continued to increase.

2.4. Processing of BMVs

Fluorescent microspheres were added into the Alg-Col solution at a concentration of 50 μg/mL to prepare fluorescently labeled BMVs. Following that, the fluorescently labeled BMVs were woven into grid or twist structures and their morphology was observed under fluorescence microscope.

2.5. Permeability and Perfusion Performance of BMVs

To test the permeability of protein in BMVs, an FITC-BSA solution (50 μg/mL) was injected into the BMVs. The permeation experiment was measured under continuous flow conditions. The syringe pump was used to inject the solution containing FITC-BSA into BMV, and pictures were taken at 3 s using a Zeiss Axiovert 200 fluorescence microscope (Carl Zeiss Inc, Thornwood, NY). The penetration distance of FITC-BSA from different BMVs was measured according to the images.

To test the perfusion capacity of the BMVs, a needle was firstly inserted into the BMVs. The red ink was then injected into the BMVs by a syringe pump, and the flow

rate is 20 μL/min. The perfusion capacity of the BMVs was tested by observing the movement of the red ink.

2.6. Cell Culture on the Hydrogels

RUVECs were seeded on different hydrogels in 24-well plates at a density of 2×10^4 cells/well. Tissue culture plates were used as the control. After 1, 3 and 5 days of culture, photos were taken through a light microscope. Cell live/dead staining was performed on day 5 using the live/dead viability/cytotoxicity kit (Invitrogen by Thermo Fisher Scientific, Eugene, OR, USA). Bone mesenchymal stem cells (BMSCs) were extracted from the tibias and femurs of male rats (6 weeks old) according to the previous method [28, 52]. The stem cell-related markers were detected by flow cytometry, and the multidirectional differentiation potential of stem cells was identified by adipogenic, chondrogenic and osteogenic induction. The BMSCs were seeded on Alg-Col composite hydrogel membrane in 24-well plates at a density of 2×10^4 cells/well. Tissue culture plates were used as the control. After 2 days of culture, the cells were stained for actin with TRITC-phalloidin（Yeasen Biotech Co., Ltd., China). The RUVECs were cultured in basal medium supplemented with 5% fetal bovine serum, 1% penicillin/streptomycin, 0.1 mg mL^{-1} heparin and 0.05 mg mL^{-1} ECGs at 37 ºC with 5 % CO_2. The BMSCs were cultured in α-MEM supplemented with 10 % fetal bovine serum and 1% penicillin/streptomycin at 37 ºC with 5 % CO_2. The images of cell live/dead staining and cytoskeleton staining were obtained using a Zeiss Axiovert 200 fluorescence microscope (Carl Zeiss Inc, Thornwood, NY).

2.7. Preparation of RUVEC-BMVs

In order to prepare cell-loaded hollow fibers, RUVECs were dispersed into a basal medium (supplemented with 5% fetal bovine serum, 1% penicillin/streptomycin, 0.1 mg mL^{-1} heparin and 0.05 mg mL^{-1} ECGs) containing 1% $CaCl_2$ and used as an inner phase fluid (F_{in}). The Alg-Col mixture was used as the outer phase fluid (F_{out}). A cell basal medium (supplemented with 5% fetal bovine serum, 1% penicillin/streptomycin,

0.1 mg mL^{-1} heparin and 0.05 mg mL^{-1} ECGs) containing 3% $CaCl_2$ was used for further crosslinking the collected fibers. After 2 min, the BMVs containing RUVECs were transferred to a culture dish containing culture medium for cell culture. After cell adhesion and proliferation on the lumen of the BMVs, RUVEC-BMVs were obtained. The whole process was carried out in an aseptic environment.

2.8. Characterization of RUVEC-BMVs

Optical images of RUVEC-BMVs were obtained by an inverted microscope (ECLIPSE Ts2, Nikon, Tokyo, Japan) at 1, 3 and 5 days. After culturing for 5 days, the cells in RUVEC-BMVs were performed s live/dead staining to investigate the cell viability through laser scanning confocal microscope (Zeiss LSM710/780, Oberkochen, Germany).

In addition, RUVECs were cultured in the BMVs (3D) and on the hydrogel at 3 and 14 days, the CD31 expression was tested via immunofluorescence. Briefly, RUVECs were fixed in 4% paraformaldehyde for 15 min and then permeabilized with 0.3% Triton X-100 in PBS for 10 min. Non-specific binding was blocked by 4% bovine serum albumin at room temperature for 1 h. After incubation with primary antibodies (rabbit anti-CD31, 1:400, Abcam, Cambridge, UK) in primary antibody dilution buffer (Beyotime, Shanghai, China) at 4 °C overnight, appropriate Cy3-labeled second antibodies (Beyotime, Shanghai, China) were incubated and DAPI for 1 hour at room temperature. Images were acquired using a fluorescence microscope.

2.9. The Content of BMP-2 and PDGF-BB in the Culture Medium

After RUVECs were cultured in the BMVs (3D) and on the hydrogel (2D), the amount of BMP-2 and PDGF-BB in the medium was investigated by ELISA assay. At given time points, the concentrations of BMP-2 and PDGF-BB in the supernatant were measured by using a commercial rat BMP-2 and PDGF-BB ELISA kits (Sangon Biotech, Shanghai, China), respectively. The optical density of each well was determined by using a microplate reader (BioTek, Vermont, USA) set to 450 nm. The

protein concentration for each sample was then calculated according to the standard curve.

2.10. *In vitro* Osteogenesis with RUVEC-BMVs

BMSCs were seeded in the lower tissue culture plate of Transwell plate at a density of 2×10^4 cells/well. They were divided into four groups. To test the effect of BMVs or RUVEC-BMVs on osteogenic differentiation of BMSCs, BMVs or RUVEC-BMVs were placed in the upper chamber of Transwell plate and to be co-cultured with BMSCs in the lower chamber. The BMV group: BMSCs were co-cultured with acellular BMVs. The RUVEC-BMV group: BMSCs were co-cultured with endothelialized BMVs (RUVEC-BMV). The preparation of osteogenesis induction medium: basal medium supplemented with 10% fetal bovine serum, 1% penicillin/streptomycin, 50 μM L^{-1} Vitamin C, 10 mM L^{-1} β-glycerophosphate and 10 nM L^{-1} dexamethasone. The BMV, RUVEC-BMV and Induced groups were cultured in the mixed medium of rat endothelial medium and osteogenesis induction medium (1:1, v/v). The Ctrl group was cultured in α-MEM medium. The medium was replaced every 2-3 days. After 7 days of culture, the cells were fixed with paraformaldehyde and stained with BCIP/NBT ALP color development kit (Beyotime, Shanghai, China) at room temperature for 30 min. After the reaction was terminated, the images were taken. After 14 days of culture, the cells were fixed with paraformaldehyde and stained with alizarin red for 30 min, and then the images were taken. After 14 days of culture, TRIzol (Invitrogen, California, USA) was used to extract the total RNA from cultured cells was detected by qPCR analysis for testing the gene expression of ALP, Col-I, OCN, OPN and Runx2. Total RNA production was measured using NanoDrop 2000 spectrophotometers (Thermo Fisher Scientific, MA, USA). One microgram of total RNA was extracted from each sample and SuperMix (Invitrogen, OR, USA) was synthesized for reverse transcription using the first strand of SuperScript III according to the manufacturer's instructions. All qPCR reactions were performed using the iTaq Universal SYBR Green Master (Bio-Rad, Hercules, CA, USA) following the manufacturer's instructions. Ten microliter

reaction components included 5 μL Master Mix, 1 μL forward and reverse primers, 1.5 μL nuclease free water and 2.5 μL cDNA template. Col-I, ALP, Runx2, OCN and OPN were selected as target gene primers. Forward and reverse primers for the selected genes are listed in Table 1. Relative expressions were calculated using the ΔΔCt method and normalized to GAPDH gene expression.

Table 1. Primers for quantitative real-time PCR.

Gene	Forward（5'-3'）	Reverse（5'-3'）	primer efficiency
ALP	TATGTCTGGAACCGCACTGAAC	CACTAGCAAGAAGAAGCCTTT	104.6%
OPN	GCGGTTCACTTTGAGGACAC	TATGAGGCGGGGATAGTCTTT	99.2%
Runx 2	ATCCAGCCACCTTCACTTACACC	GGGACCATTGGGAACTGATAG	95.3%
Col-I	CAGGCTGGTGTGATGGGATT	CCAAGGTCTCCAGGAACACC	95.1%
OCN	AACGGTGGTGCCATAGATGC	AGGACCCTCTCTCTGCTCAC	105.3%
GAPDH	GGTTGTCTCCTGCGACTTCA	TGGTCCAGGGTTTCTTACTCC	102.5%

The temperature of DNA denaturation is 95 ℃, and the primer annealing and extension temperature is 60 ℃.

After 14 days of culture, total protein of cells was extracted with RIPA Lysis Buffer (50 mM Tris, pH 7.4, 150 mM NaCl, 1% NaF and 1% Triton X-100, Beyotime, Shanghai, China). Phenylmethanesulfonyl fluoride (PMSF) was added to achieve a final concentration of 1 mM. The lysate was centrifuged at 14000 rpm at 4 °C for 15 min and cleared, and the supernatant containing protein was collected. These proteins were quantified using the BCA Protein Assay Kit (Beyotime, Shanghai, China). The extracted proteins were resolved on 10% SDS-PAGE gels and then electrically imprinted onto nitrocellulose membrane. After being enclosed with 5% skim milk at room temperature for 1-2 hours, membranes were incubated overnight with primary antibodies (rabbit anti-Col I, 1:1000, Abcam, Cambridge, UK; rabbit anti-Runx2, 1:500 ABclonal, Boston, MA, USA; rabbit anti-OCN, 1:1000, ABclonal, Boston, MA, USA) in primary antibody dilution buffer (Beyotime, Shanghai, China) at 4 °C. The horseradish peroxidase-conjugated secondary antibody was then incubated at room temperature for 1 h. The proteins were detected using autoradiography (Bio-Rad,

Hercules, CA, USA) and image J software was used to quantify the western blotting signal density.

2.11. Animal Studies

All procedures followed the NIH Guide for the Care and Use of Laboratory Animals and were approved by the Institutional Animal Care and Use Committee of Soochow University (ECSU-201700041). Fifty 10-week-old Sprague-Dawley (SD) rats were purchased and randomly divided into five groups. The rats were anesthetized with pentobarbital intraperitoneal injection and subsequently removed intracranial hair and disinfected. Then, a sagittal incision of 0.8 ~ 1.3 cm was made on the scalp of each rat to separate the skin fascia periosteum. After that, blunt dissection was performed to expose the skull. A 5 mm diameter defect was made using a bone drill at each end of the herringbone suture in the rat skull, and flush the wound liberally with Hanks balance solution while drilling. After the skull defect model was constructed, the Ctrl group was sutured directly without placing any materials. For GelMA group, the defect was filled with 15 μL GelMA solution (5 %), and was further irradiated by blue light for 30 s to cure the GelMA. In GelMA/RUVEC group, 15 μL GelMA solution (5 %) containing RUVEC (1×10^8 cells/mL) was used for bone repair. For the GelMA/RUVEC-BMV group, a RUVEC-BMV about 20 cm long was prepared, and a total of 1.5×10^6 cells were encapsulated in it. The RUVEC-BMV was cut into 1-2 mm length and all transplanted into one defect. Then 15 μL GelMA solution (5 %) was injected in the defect site and subsequently crosslinked by blue light. The initial cell number used in GelMA/RUVEC-BMV and GelMA/RUVEC groups is the same (1.5×10^6 per defect). In the GelMA/BMV group, a cell-free BMV about 20 cm long was prepared and cut into fragments (1-2 mm length), implanted into one defect and covered by GelMA hydrogel like as the GelMA/RUVEC-BMV group. The rats were sacrificed at 4 and 8 weeks respectively, and the skull was taken and fixed with 4 % paraformaldehyde solution. There are five samples in each group.

2.12. Micro-CT Analysis

The samples were analyzed using a micro-CT system (SkyScan 1176, Aartselaar, Belgium). The micro-CT was set at 50 kV, 385 mA and an aluminum filter of 1 mm. The scanned images were reconstructed using Skyscan NRecon program. The newly formed bone volume and density was also quantified.

2.13. Histology Study

The samples were decalcified with Perenyi's decalcification solution (Yuanye, Shanghai, China) for one month. The samples were then dehydrated with gradient ethanol and embedded with paraffin. Hematoxylin and eosin (H&E) staining was used to evaluate new bone formation. Anti-rat CD31 (Abcam, Cambridge, UK) was used for immunohistochemical staining.

2.14. Statistical Analysis

Quantitative data were expressed as the mean ± standard deviation. Origin Pro 8 SR4 software (OriginLab Corporation, MA, USA) and Graph prism software (GraphPad Software, CA, USA) were used to perform Student's t tests. Statistical differences between multiple sets of data were determined using one-way analysis of variance (ANOVA) tests. The LSD test was used for pairwise comparison with ANOVA. A value of $p < 0.05$ denotes statistically significant difference.

3. Results

3.1. Characterizations of Alg-Col Hydrogels

The growth of RUVECs on Alg, Col and Alg-Col is shown in Figure 1. While the cells hardly spread on the surface of Alg hydrogels (Figure 1A), they could well adhere on Alg-Col composite hydrogels. In order to check the viability of cells, live/dead staining was carried out after culturing for 5 days. The results show that only a small number of living cells on the Alg hydrogel, while there were many live cells on Col and Alg-Col hydrogels and culture plates, and almost no dead cells were found on all

hydrogels and culture plates (Figure 1B). The survival rate of cells on different hydrogels was measured using CCK-8 test after culturing for 1, 3 and 5 days, respectively. The results show that the number of cells on Alg decreased significantly compared with other groups (Figure S1). These results indicate that Alg hydrogel did not support cell adhesion and proliferation, and the addition of collagen improved the cytocompatibility of it, enabling cells to better adhere to and proliferate on it.

The hydrophilicity is an important factor affecting cell adhesion. The water contact angle of pure Alg hydrogel was less than 5° (Figure 1C). After mixing with collagen, the water contact angle of Alg-Col complex hydrogel increased to about 25°, meaning that mixing collagen and Alg decreased the hydrophilicity of Alg-Col composite hydrogels, making it closer to the hydrophilicity of culture dish (36°). Further, the mechanical properties of hydrogels were examined using compression tests. A typical strain-stress cure of Alg-Col hydrogel is shown in Figure S2. The compressive strength of Alg-Col hydrogel is 62±8 kPa, and the compression modulus is 2.83±0.14 kPa.

In order to further check the cytocompatibility of Alg-Col composite hydrogels, BMSCs were cultured on Alg-Col composite hydrogels and tissue culture plate. After one day of culture, cytoskeleton staining of the cells was performed using TRITC-phalloidin and DAPI. Clearly, BMSCs could well spread on Alg-Col composite hydrogels (Figure 1D), indicating its decent cytocompatibility.

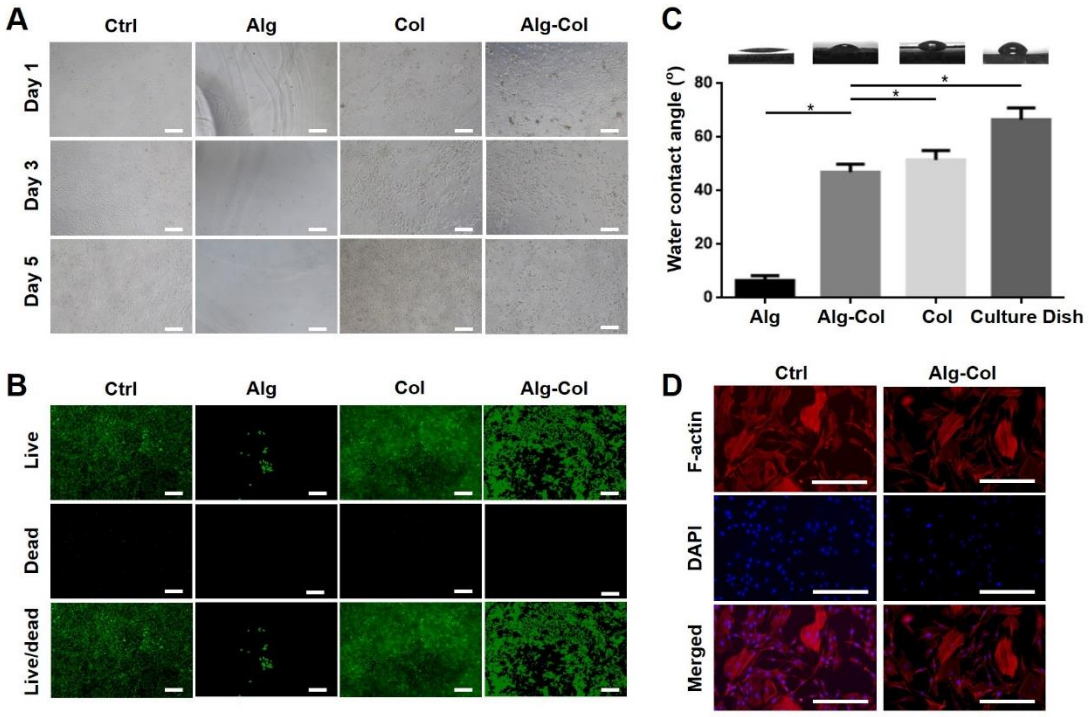

Figure 1. Cell culture on different hydrogels. Optical microscopy (A) and live/dead staining (B) images of RUVECs on Alg (20 mg/mL), Col (3 mg/mL) and Alg-Col (20 mg/ml, 2 mg/mL) hydrogels and tissue culture plate. Green represents live cells and red represents dead cells. (C) The water contact angle of different hydrogels and tissue culture plate (n=3). (D) Representative images of cytoskeleton/nuclei staining of BMSCs on Alg-Col hydrogels and culture plate. *, $p < 0.05$. Scale bars, 400 μm.

3.2. Fabrication and Characterizations of BMVs

A two-phase microfluidic device was used in this study to prepare the BMVs. The inner phase fluid was calcium chloride solution, and the outer phase fluid was a mixed solution containing sodium alginate and collagen. Ionic crosslinking occurred rapidly after sodium alginate and calcium ions contact with each other. The outer layer rapidly solidified into a gel and formed hollow fibers immediately. The moderately cured hollow fibers were collected in a culture dish containing calcium chloride and further crosslinked to form stable hollow fibers which were BMV. BMVs with various wall thicknesses were prepared by adjusting the flow rate of internal and external phases, respectively (Figure 2A). When the flow rate of outer phase was 0.1 mL/min and the

flow rate of inner phase was 0.3 mL/min, the BMV wall thickness was 100 μm ± 20 μm. When the flow rate of outer phase was maintained at 0.1 mL/min and the flow rate of inner phase was reduced to 0.1 mL/min, the BMV wall thickness increased to about 150 μm ± 20 μm. In addition, when the flow rate of outer phase was maintained at 0.1 mL/min and the flow rate of inner phase further decreased to 0.05 mL/min, the wall thickness continued to increase. SEM images exhibit the different wall thicknesses of BMVs (Figure 2B). The BMV microfibers had enough strength for further processing. As shown in Figure 2C, the BMVs could be woven into a grid structure or a multi-strand twist structure. These results show that the BMVs had considerable size adjustability and processability.

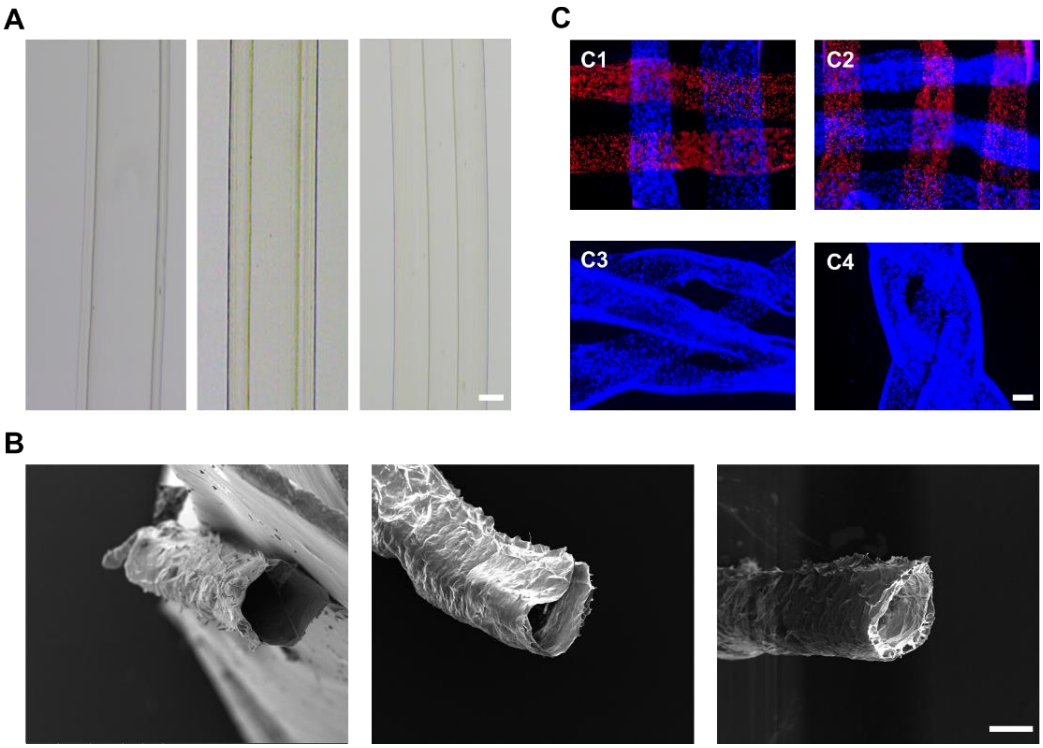

Figure 2. Microfluidic fabrication of Alg-Col BMVs. (A) Microscopy images of BMVs with different inner diameters. The flow rate of outer phase was 0.1 mL/min and the flow rate of inner phase was 0.3, 0.1 and 0.05 mL/min, respectively, from left to right. (B) SEM images of hollow microfibers with different wall thickness. (C) Fluorescence microscopy images of different woven architectures of hollow microfibers. (C1&C2) grid structure; (C3&C4) twist structure. Scale bars, 200 μm.

The permeation and perfusion properties are two of the most important features of blood vessels. The FITC-BSA was injected into BMVs prepared with different conditions. Results showed that the permeation of BMVs varies with the concentration of alginate and the degree of crosslinking (Figure 3A). FITC-BSA is not permeable easily in high concentration and crosslinking of BMVs, but easily permeable in low concentration and crosslinking BMVs. When the concentration of alginate and $CaCl_2$ solutions are 1 %, BMVs show the lowest crosslinking degree, and the fastest permeable rate, and the penetration distance is about 600 ± 20 μm. When the concentration of alginate and $CaCl_2$ are 3 %, BMVs show the highest concentration and crosslinking degree, and BSA is almost impermeable. In order to ensure the exudation of factors contributing to bone formation, low-concentration alginate was used to prepare BMVs in this study. The perfusion property could be reflected by the flow of red ink in the microfiber. As shown in Figure 3B, the red ink could be injected into the BMV and freely flow through the channel. Perfusion results showed that BMV obtained by this method could achieve nutrient delivery. These results demonstrate that the BMVs contain permeability and perfusibility, which may mimetic the function of native blood vessels.

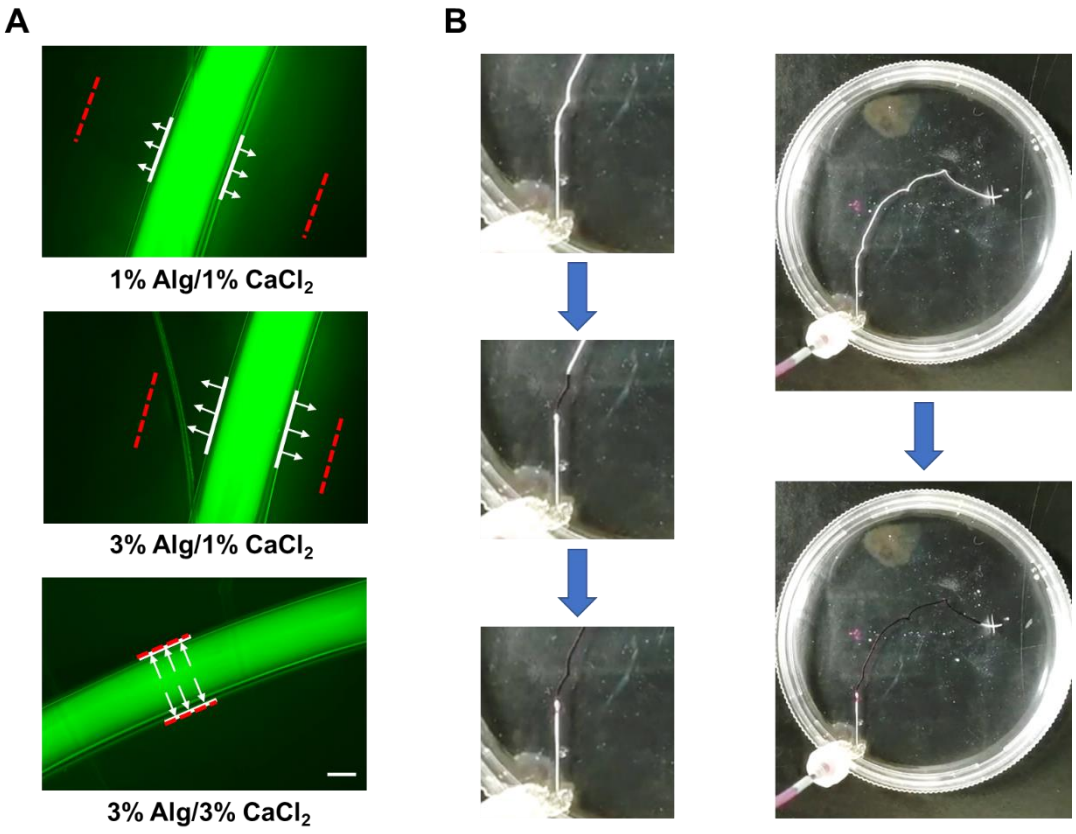

Figure 3. Perfusion and permeation of BMVs. (A) Permeation of FITC-BSA from the hollow alginate microfibers (white lines and red dotted lines represent starting and ending points, respectively, and white arrows represent the direction of penetration). (B) Perfusion of red ink in the channels of hollow microfibers. Scale bars, 200 μm.

3.3. Characterizations of RUVEC-BMVs

RUVECs were loaded into hollow channels of microfibers to form an endodermis, mimicking the lumen of a blood vessel. RUVECs were dispersed into complete medium containing $CaCl_2$, and then crosslinked with the external phase through coaxial needles to form RUVEC-BMVs. Clearly, RUVECs proliferated well on the inner wall of BMV and eventually grew into a cell-loaded BMV (RUVEC-BMV) (Figure 4A). In order to further check the status of cells, live/dead staining of BMVs at day 5 was performed. As shown in Figure 4B, few dead red cells were observed. Moreover, RUVECs interconnected with each other to form a layer of cells at day 5, resembling the endothelium of blood vessels. The cross-section view clearly shows a lumen structure

of RUVEC-BMV, with a RUVEC layer at the inner wall (Figure 4B). These results indicate that endothelialized BMVs had been successfully prepared. The CD31 expression of RUVECs in RUVEC-BMVs (3D) or cultured on the hydrogel (2D) at 3 and 14 days is shown in Figure 5. Compared with 2D cell culture, 3D culture is more conducive to enhance the expression of CD31 in endothelial cells.

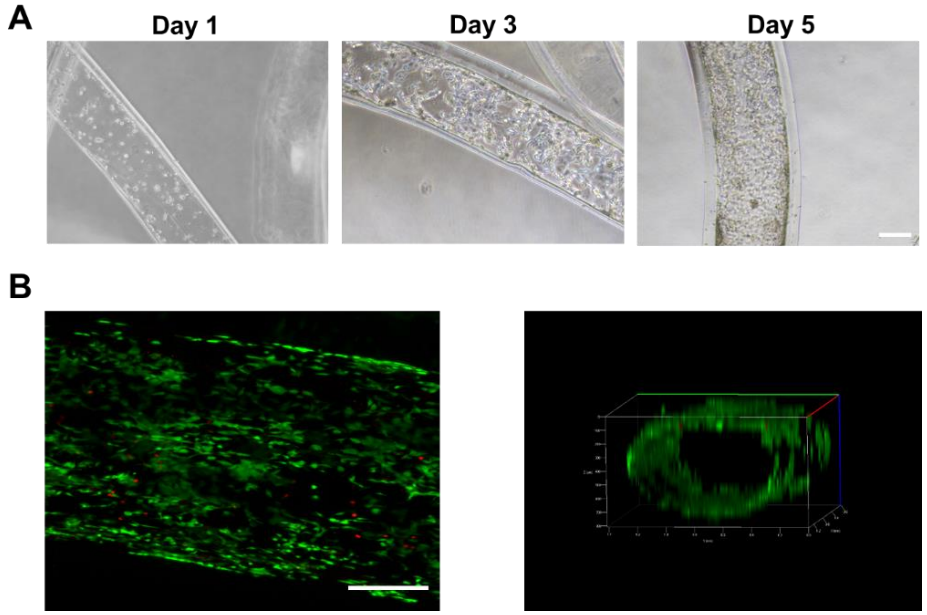

Figure 4. Characterizations of RUVEC-BMVs. (A) Optical microscopy images of RUVEC-BMVs after culturing for 1, 3, 5 days, respectively. (B) CLSM images of live/dead staining for RUVEC-BMVs after culturing for 5 days. Green stands for live cell and red stands for dead cell. Scale bars, 200 μm.

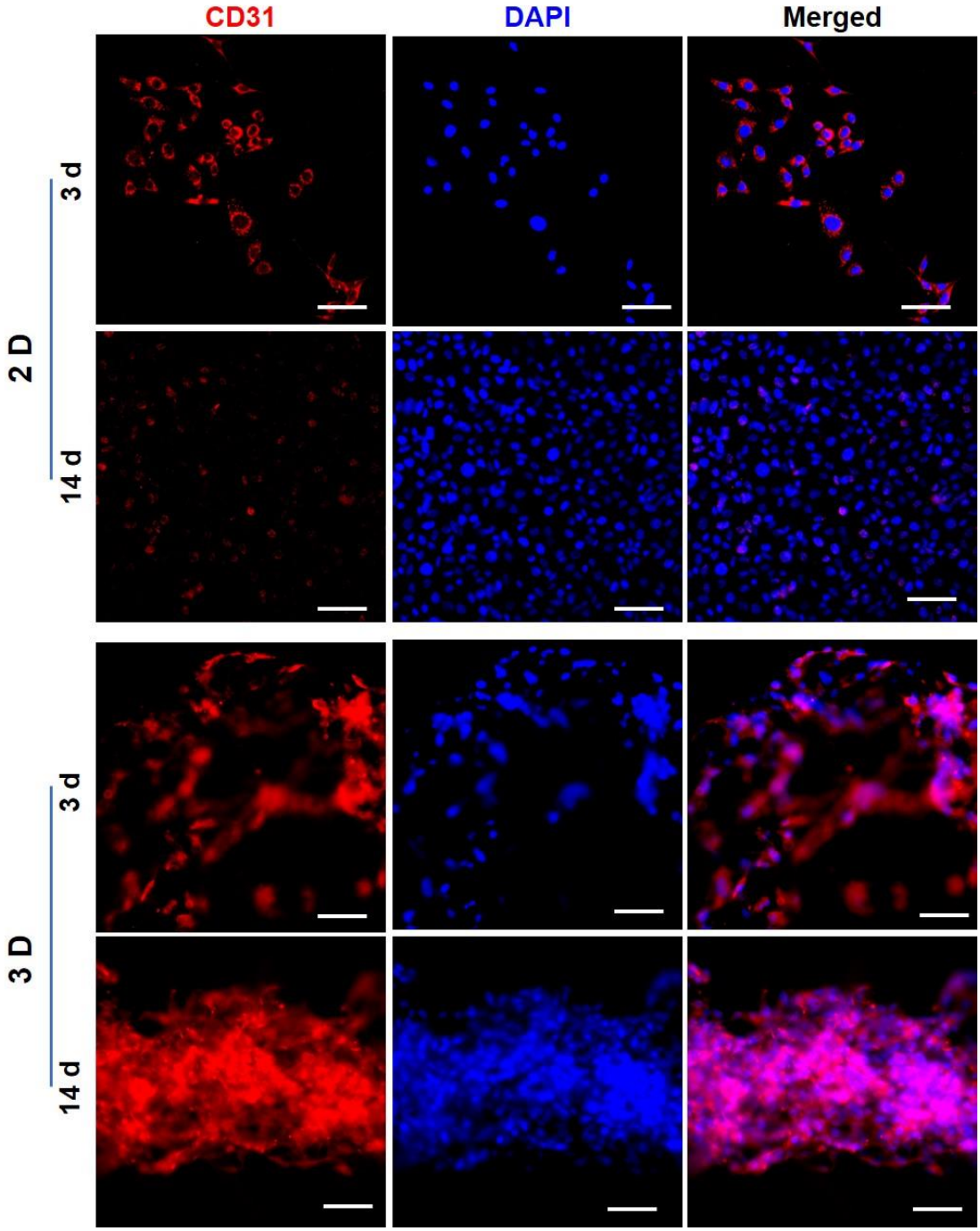

Figure 5. The expression of CD31 in RUVECs on RUVEC-BMVs (3D) or cultured on the hydrogel (2D) at 3 and 14 days, respectively. Scale bars, 50 μm.

3.4. Secretion of BMP-2 and PDGF-BB in the Culture Medium

The same number of RUVECs were encapsulate into the RUVEC-BMVs or seeded on the hydrogel and culture for 21 days. Through detecting the amount of BMP-2 and PDGF-BB in the culture medium, it is found that both the content of BMP-2 and

PDGF-BB increases with culture time (Figure 6). In addition, the amount of BMP-2 and PDGF-BB is higher in the medium of RUVEC-BMVs (3D) than the RUVECs cultured on the hydrogel (2D).

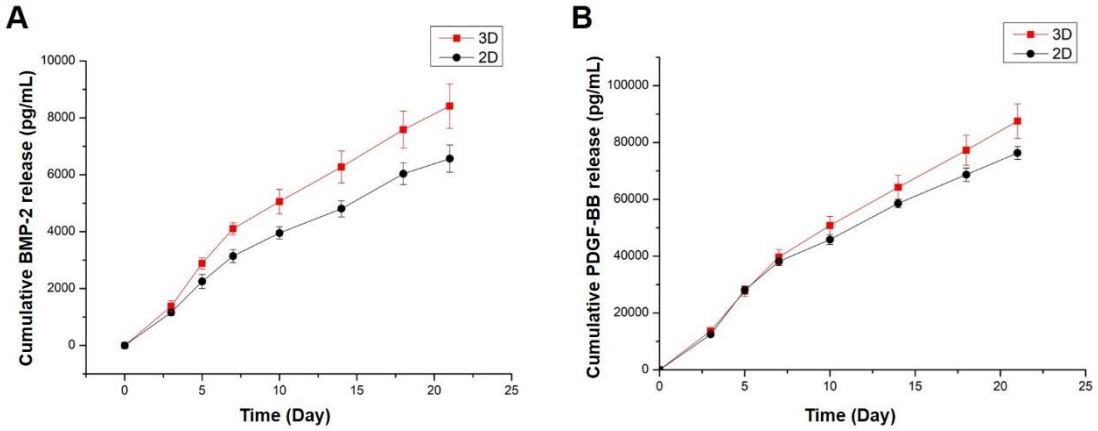

Figure 6. The content of BMP-2 (A) and PDGF-BB (B) in the culture medium of RUVEC-BMVs (3D) or RUVEC cultured on the hydrogel (2D) (n=5).

3.5. Effect of RUVEC-BMVs on the Osteogenic Differentiation of BMSCs

The stem cell characteristics of extracted BMSCs were identified. According to the results of Figure S3, the BMSCs can express the stem cell-related markers, and show the multidirectional differentiation potential through adipogenic, chondrogenic and osteogenic induction. In order to verify the effect of biomimetic vessels on the osteogenic differentiation of BMSCs, ALP staining and alizarin red staining were performed to detect ALP activity and calcium deposition, respectively. After 7 days of culture, the RUVEC-BMV group shows the highest ALP expression (Figure 7A). However, there is no apparent difference in ALP expression between the Induced group and BMV group. In order to observe the calcium deposition of cells, BMSCs were stained with alizarin red after 14 days of culture. The results of alizarin red staining further demonstrate the enhanced bone forming ability of endothelialized BMVs (Figure 7B). Similar to the results of ALP staining, the RUVEC-BMV group shows the most calcium nodules than other groups. The content of calcium nodules in BMV group is similar to that of Induced group. In order to further verify the effect of endothelialized

BMVs on the formation of calcium nodules in BMSCs, perchloric acid was applied to quantitatively analyze the results of alizarin red staining (Figure 7C). It is found that the quantitative results are consistent with the staining results. These results indicate that BMSCs have a very weak ability to produce calcium nodules under control condition, and the formation of calcium nodules can be accelerated only through induction. RUVEC-BMVs, but not BMVs, significantly accelerated the formation of calcium nodules in BMSCs.

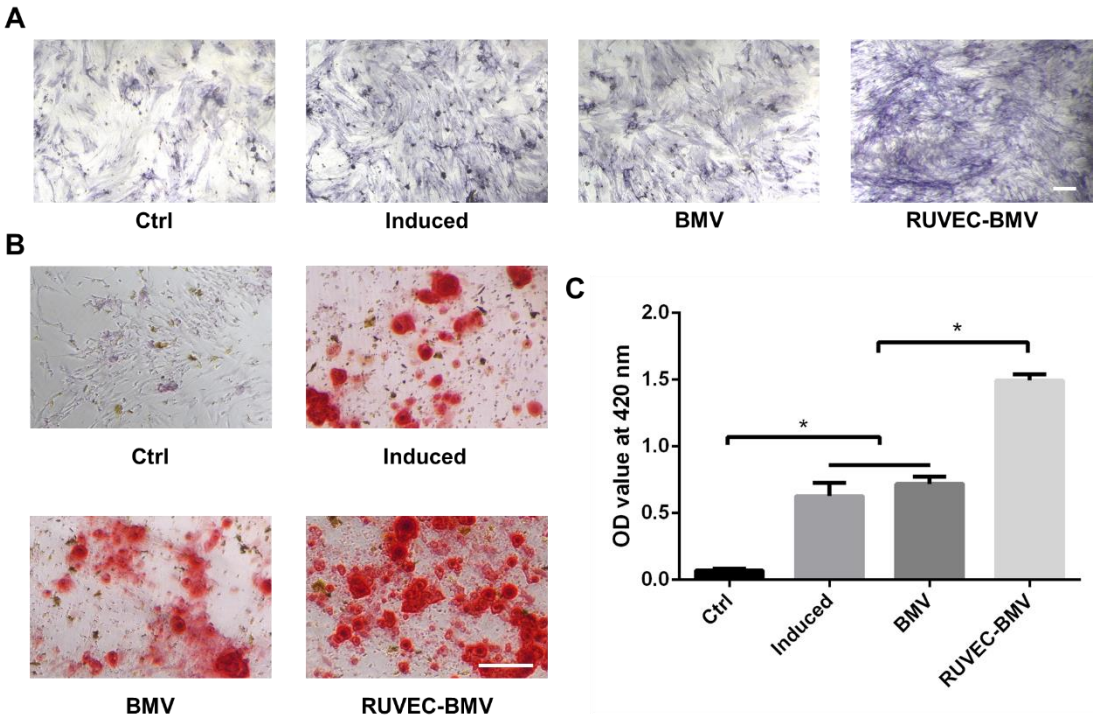

Figure 7. In vitro osteogenesis of BMSCs cultured with supplement of BMVs. (A) ALP staining of the BMSCs after osteogenic induction for 7 days and (B) Alizarin red staining of the BMSCs after osteogenic induction for 14 days. (C) Quantitative analysis of alizarin red staining. *, $p < 0.05$ (n=5). Scale bars, 200 μm.

The expression of genes related to osteogenesis at 14 days was detected by qRT-PCR. The results show that the gene expression of Col-I, ALP, Runx2, OPN and OCN in BMV group is similar to that in Induced group (Figure 8A-E). The expressions of Col-I, ALP, Runx2, OPN and OCN in RUVEC-BMV group are higher than that in the BMV group. The expressions of genes related to osteogenesis in the Induced group,

BMV group and RUVEC-BMV group are all higher than Ctrl group. Meanwhile, RUVEC-BMV group shows the highest expression of osteogenic genes. Western blot analysis also confirms that the protein expressions of Col-I, Runx2 and OCN are significantly enhanced in the RUVEC-BMV group compared with other groups (Figure 8F-I).

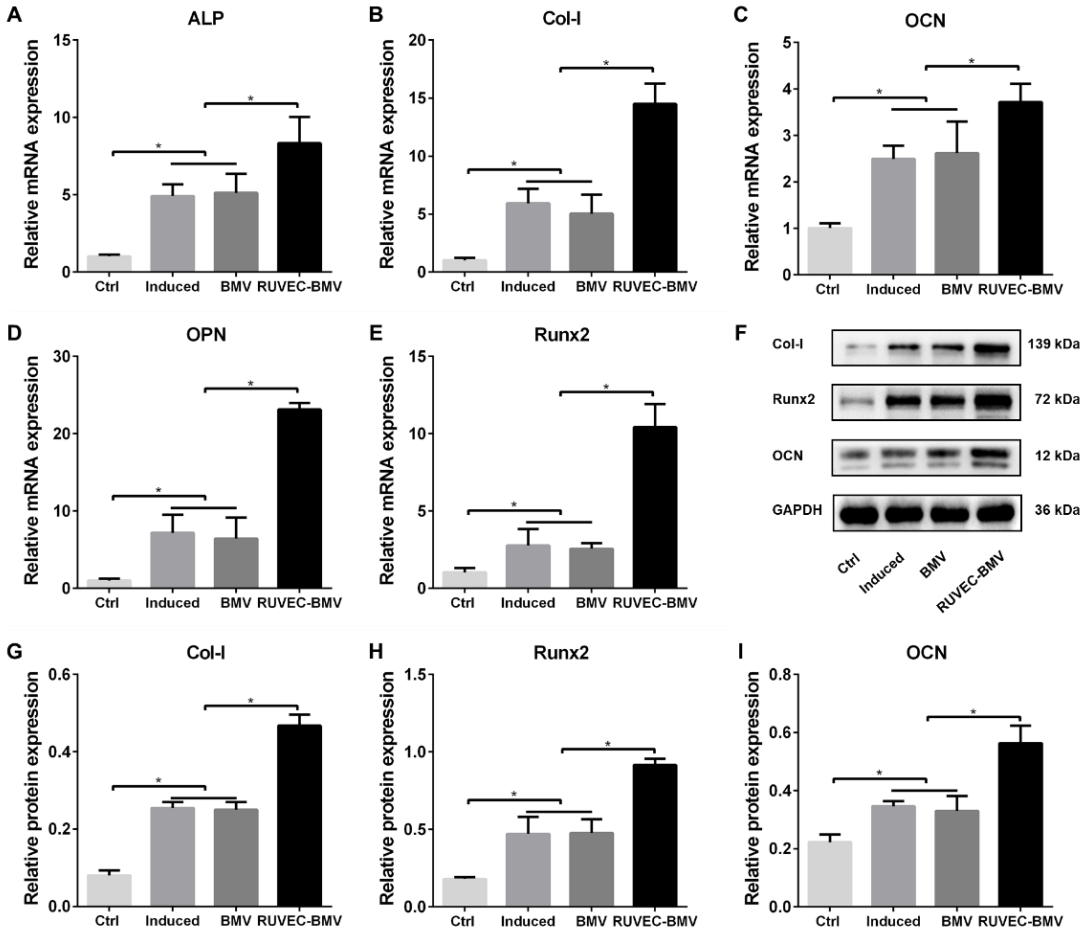

Figure 8. Expression of osteogenesis-related genes and secretion of proteins in BMSCs *in vitro*. (A-E) Gene expression of ALP, Col-I, OCN, OPN and Runx2, respectively. GAPDH was used as the housekeeping gene. (F-I) Western blot analysis. *, $p < 0.05$ (n=5).

3.6. Repair of Rat Skull Defects Using RUVEC-BMVs

Micro-CT was used to evaluate the effect of endothelialized biomimetic vessels on rat skull repair. After 4 weeks, micro-CT results show that only a small amount of bone is formed in the skull defect of the Ctrl group (Figure 9A-B). After 4 weeks, the

rate of new bone formation in GelMA group, GelMA/BMV group, GelMA/RUVEC group and GelMA/RUVEC-BMV group reach 7.82%, 7.27%, 12.72% and 21.12%, respectively, which are significantly higher than those in the Ctrl group. The results indicate that the implantation of material promotes bone regeneration. GelMA group and GelMA/BMV group show a small amount of new bone formation without significant difference. The result shows that the biomimetic blood vessel without carrying cells had no obvious effect on bone formation. On the other hand, the GelMA/RUVEC group shows more bone formation than that of GelMA group and GelMA/BMV groups, which indicates that the addition of RUVECs improves bone regeneration. Compared with GelMA/RUVEC group, GelMA/RUVEC-BMV group shows significantly more new bone formation (almost doubled the amount of the bone formation). These results indicate that GelMA hydrogels have a certain effect of promoting bone repair. The RUVECs dispersed in the GelMA hydrogels also enhanced bone repair. However only the RUVECs that form the lumen in the biomimetic blood vessel play the strongest role in promoting bone repair. The BV/TV value of GelMA/RUVEC-BMV group is the highest than other groups at both 4 weeks and 8 weeks. H&E staining further confirms these results. Compared with control, GelMA, GelMA/BMV and GelMA/RUVEC groups, GelMA/RUVEC-BMV group has the best bone formation at 4 and 8 weeks (Figure 9C). The new blood vessels represented by CD31 immunohistochemical staining (Figure S4). New blood vessels form in the implanting site of all the groups. However, the vascularization in GelMA/RUVEC-BMV group is more obvious than other groups. Some big vessels are observed in the GelMA/RUVEC-BMV group both at 8 weeks.

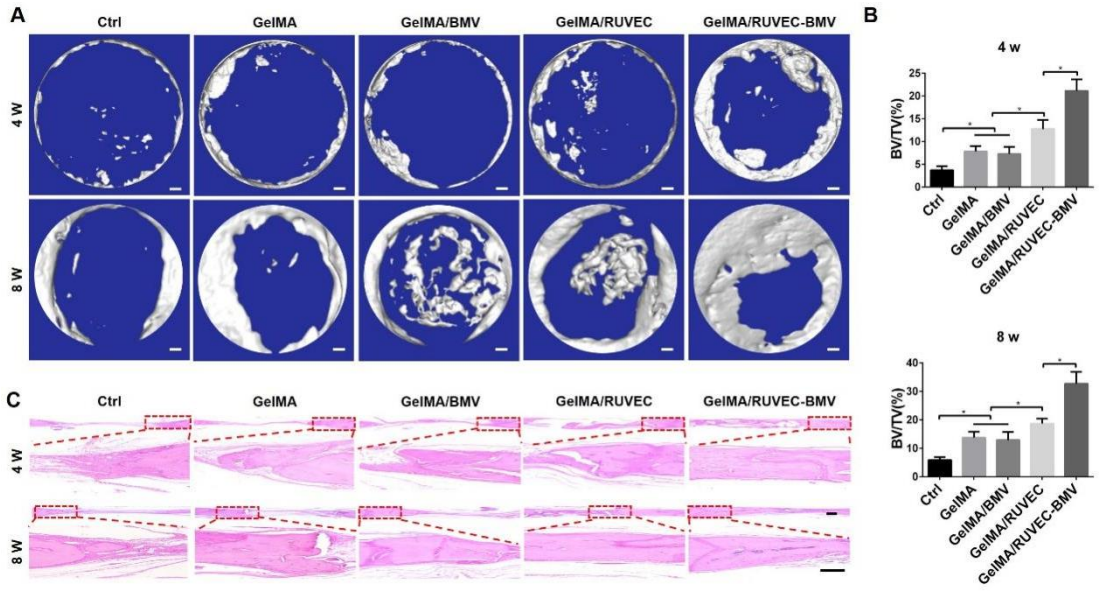

Figure 9. The repair of rat skull defects using different materials at 4 and 8 weeks, respectively. (A) Micro-CT images. (B) BV/TV values measured by micro-CT. (C) H&E staining. *, $p < 0.05$ (n=5). Scale bars, 400 μm.

4. Discussion

Tissue engineering is a technique that uses bioactive substances to repair or regenerate tissue through tissue engineered constructs [53]. One of the biggest limitations in tissue engineering is that regenerated organs or tissues do not have enough blood supply to maintain tissue viability during the initial stage after transplantation [54, 55]. Angiogenesis plays an important role in tissue engineering [56]. Before the formation of a network of blood vessels, an implant must rely on diffusion to provide nutrients and remove wastes from the body [57, 58]. The nutritional deficiencies at the implant site, may cause improper integration of the implants or even complete loss of function. *In vitro* constructing BMVs provides a good nutrition delivery strategy for organ or tissue repair *in vivo* [59].

In recent years, many methods have been explored for the preparation of artificial blood vessels and large-diameter (> 6 mm) BMVs which are ideal for the purpose of establishment of microvascular network for tissue perfusion. However, further research

is still needed for the preparation of small-diameter (< 6 mm) blood vessels. Compared with traditional methods such as 3D printing [60], electrospinning [61] and mold method [60 ,62], microfluidic technology has the advantages of time saving and size control. However, microfluidic technology could prepare the complex vascular structure, provide customizable geometric and chemical complexity for fiber, and can produce continuous long fiber, which make it become a new direction for vascularization tissue engineering [46, 63, 64]. Microfibers with various size, shape and composition can be prepared by microfluidic technology. For example, Asthana et al. successfully prepared sodium alginate microfibers with hollow structure on PDMS microfluidic chip by using the ion crosslinking reaction between sodium alginate and calcium ions [13].

The preparation of hollow hydrogel fibers using microfluidic technology has become a prime concern in recent years [65]. In our previous study, the hollow biomimetic vascular structure carrying human umbilical vein endothelial cells have been successfully prepared [51, 59]. In this study, the BMVs with different wall thickness were obtained used biocompatible materials (Figure 1) via adjusting the flow rate (Figure 2). The SEM images clearly show the hollow structure and surface morphology of the BMVs (Figure 2B). It is well known that Alg hydrogels are not sufficient to provide a favorable microenvironment for cells due to the lack of bioactive sites [66]. Alginate alone lacks cell adhesion sites, so we observed fewer cells (dead or living cells) in Alg group. Because alginate lacks the site of cell adhesion, although it has no cytotoxicity, it does not support cell adhesion and proliferation too. Studies have been carried out to improve its biocompatibility by grafting cell adhesion peptide and other methods [67-69]. However, these methods are time-consuming, and the preparation processes are complicated. In order to prepare cell-laden biomimetic blood vessels, Alg hydrogels have been modified with collagen (Figure 1). Collagen is one of the most widely used biomaterials due to its excellent biological properties and physicochemical properties [9]. As shown in Figure 2B and Figure S1, the addition of

collagen improved the contact angle of alginate, making it comparable to the culture dish and more conducive to cell adhesion.

The ability to process and assemble BMVs into 3D vascular network is also an important consideration for better application in tissue engineering [70]. In order to meet the needs of different environments in the body, BMVs are needed to assemble into different structures [71, 72]. However, due to the weak mechanical strength of most hydrogels, the assembling of BMVs is difficult. Because the BMVs were very small and there was no suitable method to detect their mechanical properties. Therefore, we measured the mechanical properties of Alg-Col hydrogels, which were used to build BMVs. It was found that the compressive strength of hydrogel is 62±8 kPa, and the compression modulus is 2.83±0.14 kPa. The hydrogels are relatively strong, and the results in Figure 2 also show that the BMVs can be woven into different structures while maintaining the tubular structure. In order to demonstrate the great potential of the BMVs to create three-dimensional biomimetic tissue, BMVs were assembled by braiding. Several complex 3D architectures were created using BMVs containing fluorescent spheres. In addition, as the biomimetic blood vessels, the permeation and perfusion are also important. The results of this study show that the permeation of BMVs decreases with the concentration of alginate and the degree of crosslinking (Figure 3A). The red ink exhibits good flow ability in the channel of BMVs. With the method of this study, the drugs can also be easily encapsulated into the fiber tubes, then the drugs can be released slowly to promote tissue regeneration. The above results demonstrate that the BMVs have good processability, permeation and perfusion properties, which may have potential application in biomedical field.

In addition to the structural resemblance of blood vessel, vascular ECs are also needed to be considered [71]. ECs not only provide a smooth luminal surface to conduct blood flow, but also play a vital role in maintaining vascular homeostasis, including vessel wall permeation, vascular tone, luminal patency and blood coagulation [73-75]. However, bioengineering of endothelialized microvessels presents a big challenge [76]. In this study, we dispersed RUVECs in a medium containing calcium chloride as the

inner phase to obtain RUVEC-BMVs via a single step microfluidic technology. Following a few days of culture, RUVECs proliferated well on the luminal surface of the tube, and formed a complete endothelium in the BMVs (Figure 4). Live/dead staining shows that the cell survival rate is over 99%. BMVs have hollow and tubular structures, which can simulate the in vivo 3D environment of RUVEC, help the regular arrangement of cells, form lumen structure and maintain cell phenotype. Therefore, while the cell density was similar in 2D and 3D culture of cells, our results show that compared with 2D culture, 3D culture better enhanced the expression of CD31 in ECs (Figure 5).

In this study, to verify the effect of RUVEC-BMVs on osteogenesis, RUVEC-BMVs were co-cultured with BMSCs to simulate the in vivo environment. As expected, there was more ALP expression and calcium nodules formation in RUVEC-BMV group compared with other groups (Figure 7). Moreover, the expressions of osteogenic genes and proteins in RUVEC-BMV group are also higher than others (Figure 8). These results confirm that endothelialized BMVs contribute to osteogenesis. In addition, we also explored the paracrine effect of BMVs and found that compared with 2D culture, 3D culture promoted the secretion of osteogenic and angiogenic factors in RUVECs (Figure 6). This might partially be the reason why GelMA/RUVEC-BMV promoted osteogenesis and showed better bone repair effect than GelMA/RUVEC alone. The bone formation ability of the biomimetic vessels in vivo was further evaluated. For the in vivo implantation, a BMV about 20 cm long was cut into short segment and implanted in the skull. Because we found long BMVs were unevenly distributed in the defect area. Compared with other groups, the RUVEC-BMV group shows the best new bone formation at 8 weeks after implantation (Figure 9). In addition to thicker trabecular bone formation, new bone began to grow from the edge of the defect to the center. This is consistent with the results of in vitro osteogenesis. The new blood vessels were also observed in the implanted site. However, no remaining microvessels were found due to the fast degradation of the BMVs. Moreover, a number of large blood vessels have been observed in the GelMA/RUVEC-BMV group, which further

demonstrates the potential of RUVEC-BMVs to promote vascularization in vivo. Therefore, findings from both in vitro and in vivo studies have confirmed that the endothelialized BMVs promoted bone regeneration. It is worth noting that no BMVs were found to be linked to the vascular system in our in vivo studies. Such a limitation will be specially addressed in our further study.

5. Conclusion

In this study, we have successfully developed a microfluidics-based method to construct endothelialized BMVs. The BMVs could be easily prepared into various sizes simply by adjusting the flow rate, and showed considerable perfusion and penetration properties. The BMVs are conducive to the maintenance of endothelial cell phenotype and promote the secretion of BMP-2 and PDGF-BB. Moreover, the endothelialized BMVs had better osteogenic potential than non-endothelialized BMVs. Together, findings from this study suggest that the use of endothelialized BMVs may promote vascularization in bone tissue engineering. Such a vascularization technology might also be adopted in engineering other tissues to promote in situ tissue repair/regeneration.

Acknowledgments

The authors are grateful to the funding support from National Natural Science Foundation of China (81925027, 82111530157, 31872748, 32171350), Natural Science Foundation of Jiangsu Province (BK20191150), Jiangsu Provincial Special Program of Medical Science (BL2012004), and the Priority Academic Program Development program of Jiangsu Higher Education Institutions.

References

[1] R.D. Prisby, Mechanical, hormonal and metabolic influences on blood vessels, blood flow and bone, J Endocrinol 235 (3) (2017) R77-R100.

[2] Y. Peng, S. Wu, Y. Li, J.L. Crane, Type H blood vessels in bone modeling and remodeling, Theranostics 10 (1) (2020) 426-436.

[3] T. Niedzwiedzki, J. Filipowska, Bone remodeling in the context of cellular and systemic

regulation: the role of osteocytes and the nervous system, J Mol Endocrinol 55 (2) (2015) R23-36.

[4] B. Huang, W. Wang, Q. Li, Z. Wang, B. Yan, Z. Zhang, L. Wang, M. Huang, C. Jia, J. Lu, S. Liu, H. Chen, M. Li, D. Cai, Y. Jiang, D. Jin, X. Bai, Osteoblasts secrete Cxcl9 to regulate angiogenesis in bone, Nat Commun 7 (2016) 13885.

[5] Y. Zheng, Y. Yang, Y. Deng, Dual therapeutic cobalt-incorporated bioceramics accelerate bone tissue regeneration, Mater Sci Eng C Mater Biol Appl 99 (2019) 770-782.

[6] M. Orth, M.A.B. Altmeyer, C. Scheuer, B.J. Braun, J.H. Holstein, D. Eglin, M. D'Este, T. Histing, M.W. Laschke, T. Pohlemann, M.D. Menger, Effects of locally applied adipose tissue-derived microvascular fragments by thermoresponsive hydrogel on bone healing, Acta Biomater 77 (2018) 201-211.

[7] W. Liu, G. Zhang, J. Wu, Y. Zhang, J. Liu, H. Luo, L. Shao, Insights into the angiogenic effects of nanomaterials: mechanisms involved and potential applications, J Nanobiotechnology 18 (1) (2020) 9.

[8] Y. Yan, H. Chen, H. Zhang, C. Guo, K. Yang, K. Chen, R. Cheng, N. Qian, N. Sandler, Y.S. Zhang, H. Shen, J. Qi, W. Cui, L. Deng, Vascularized 3D printed scaffolds for promoting bone regeneration, Biomaterials 190-191 (2019) 97-110.

[9] C. Piard, H. Baker, T. Kamalitdinov, J. Fisher, Bioprinted osteon-like scaffolds enhance in vivo neovascularization, Biofabrication 11 (2) (2019) 025013.

[10] A. Morss Clyne, S. Swaminathan, A. Diaz Lantada, Biofabrication strategies for creating microvascular complexity, Biofabrication 11 (3) (2019) 032001.

[11] E.C. Watson, R.H. Adams, Biology of Bone: The Vasculature of the Skeletal System, Cold Spring Harb Perspect Med 8 (7) (2018) a031559.

[12] T. Toros, K. Ozaksar, Reconstruction of traumatic tubular bone defects using vascularized fibular graft, Injury (2019) 30475-30479.

[13] X. Sun, J. Wu, B. Qiang, R. Romagnuolo, M. Gagliardi, G. Keller, M.A. Laflamme, R.K. Li, S.S. Nunes, Transplanted microvessels improve pluripotent stem cell-derived cardiomyocyte engraftment and cardiac function after infarction in rats, Sci Transl Med 12 (562) (2020) eaax2992.

[14] J.R. Perez, D. Kouroupis, D.J. Li, T.M. Best, L. Kaplan, D. Correa, Tissue Engineering and Cell-Based Therapies for Fractures and Bone Defects, Front Bioeng Biotechnol 6 (2018) 105.

[15] S. Govender, C. Csimma, H.K. Genant, A. Valentin-Opran, Y. Amit, R. Arbel, H. Aro, D. Atar, M. Bishay, M.G. Borner, P. Chiron, P. Choong, J. Cinats, B. Courtenay, R. Feibel, B. Geulette, C. Gravel, N. Haas, M. Raschke, E. Hammacher, D. van der Velde, P. Hardy, M. Holt, C. Josten, R.L. Ketterl, B. Lindeque, G. Lob, H. Mathevon, G. McCoy, D. Marsh, R. Miller, E. Munting, S. Oevre, L. Nordsletten, A. Patel, A. Pohl, W. Rennie, P. Reynders, P.M. Rommens, J. Rondia, W.C. Rossouw, P.J. Daneel, S. Ruff, A. Ruter, S. Santavirta, T.A. Schildhauer, C. Gekle, R. Schnettler, D. Segal, H. Seiler, R.B. Snowdowne, J. Stapert, G. Taglang, R. Verdonk, L. Vogels, A. Weckbach, A. Wentzensen, T. Wisniewski, Recombinant human bone morphogenetic protein-2 for treatment of open tibial fractures: a prospective, controlled, randomized study of four hundred and fifty patients, J Bone Joint Surg Am 84 (12) (2002) 2123-2134.

[16] S.J. Kim, Y.W. Shin, K.H. Yang, S.B. Kim, M.J. Yoo, S.K. Han, S.A. Im, Y.D. Won, Y.B. Sung, T.S. Jeon, C.H. Chang, J.D. Jang, S.B. Lee, H.C. Kim, S.Y. Lee, A multi-center, randomized, clinical study to compare the effect and safety of autologous cultured osteoblast (Ossron)

injection to treat fractures, BMC Musculoskelet Disord 10 (2009) 20.
[17] L. Yu, Y. Cai, H. Wang, L. Pan, J. Li, S. Chen, Z. Liu, F. Han, B. Li, Biomimetic bone regeneration using angle-ply collagen membrane-supported cell sheets subjected to mechanical conditioning, Acta Biomater 112 (2020) 75-86.
[18] Y. Wang, W. Zhang, Q. Yao, Copper-based biomaterials for bone and cartilage tissue engineering, J Orthop Translat 29 (2021) 60-71.
[19] J.R. Garcia, A.Y. Clark, A.J. Garcia, Integrin-specific hydrogels functionalized with VEGF for vascularization and bone regeneration of critical-size bone defects, J Biomed Mater Res A 104 (4) (2016) 889-900.
[20] C.S. Ong, P. Yesantharao, C.Y. Huang, G. Mattson, J. Boktor, T. Fukunishi, H. Zhang, N. Hibino, 3D bioprinting using stem cells, Pediatr Res 83 (1-2) (2018) 223-231.
[21] M. Orth, A.K. Shenar, C. Scheuer, B.J. Braun, S.C. Herath, J.H. Holstein, T. Histing, X. Yu, W.L. Murphy, T. Pohlemann, M.W. Laschke, M.D. Menger, VEGF-loaded mineral-coated microparticles improve bone repair and are associated with increased expression of epo and RUNX-2 in murine non-unions, J Orthop Res 37 (4) (2019) 821-831.
[22] X. Zheng, X. Zhang, Y. Wang, Y. Liu, Y. Pan, Y. Li, M. Ji, X. Zhao, S. Huang, Q. Yao, Hypoxia-mimicking 3D bioglass-nanoclay scaffolds promote endogenous bone regeneration, Bioact Mater 6 (10) (2021) 3485-3495.
[23] H. Yu, X. Zeng, C. Deng, C. Shi, J. Ai, W. Leng, Exogenous VEGF introduced by bioceramic composite materials promotes the restoration of bone defect in rabbits, Biomed Pharmacother 98 (2018) 325-332.
[24] S. Zhang, J. Chen, Y. Yu, K. Dai, J. Wang, C. Liu, Accelerated bone regenerative efficiency by regulating sequential release of BMP-2 and VEGF and synergism with sulfated chitosan, ACS Biomater Sci Eng 5 (4) (2019) 1944-1955.
[25] R. Zhang, J. Liu, S. Yu, D. Sun, X. Wang, J. Fu, J. Shen, Z. Xie, Osteoprotegerin (OPG) promotes recruitment of endothelial progenitor cells (EPCs) via CXCR4 signaling pathway to improve bone defect repair, Med Sci Monit 25 (2019) 5572-5579.
[26] B.S. Ding, Z. Cao, R. Lis, D.J. Nolan, P. Guo, M. Simons, M.E. Penfold, K. Shido, S.Y. Rabbany, S. Rafii, Divergent angiocrine signals from vascular niche balance liver regeneration and fibrosis, Nature 505 (7481) (2014) 97-102.
[27] S. Han, C. Tan, J. Ding, J. Wang, A. Ma'ayan, V. Gouon-Evans, Endothelial cells instruct liver specification of embryonic stem cell-derived endoderm through endothelial VEGFR2 signaling and endoderm epigenetic modifications, Stem Cell Res 30 (2018) 163-170.
[28] L. Li, J. Li, Q. Zou, Y. Zuo, B. Cai, Y. Li, Enhanced bone tissue regeneration of a biomimetic cellular scaffold with co-cultured MSCs-derived osteogenic and angiogenic cells, Cell Prolif 52 (5) (2019) e12658.
[29] R. Junka, K. Quevada, X. Yu, Acellular polycaprolactone scaffolds laden with fibroblast/endothelial cell-derived extracellular matrix for bone regeneration, J Biomed Mater Res A 108 (2) (2020) 351-364.
[30] G.M. Price, K.H. Wong, J.G. Truslow, A.D. Leung, C. Acharya, J. Tien, Effect of mechanical factors on the function of engineered human blood microvessels in microfluidic collagen gels, Biomaterials 31 (24) (2010) 6182-6189.
[31] A. Hasan, A. Paul, A. Memic, A. Khademhosseini, A multilayered microfluidic blood vessel-like structure, Biomed Microdevices 17 (5) (2015) 88.

[32] D.B. Kolesky, R.L. Truby, A.S. Gladman, T.A. Busbee, K.A. Homan, J.A. Lewis, 3D bioprinting of vascularized, heterogeneous cell-laden tissue constructs, Adv Mater 26 (19) (2014) 3124-3130.
[33] Q. Hu, C. Wu, H. Zhang, Preparation and optimization of a biomimetic triple-layered vascular scaffold based on coaxial electrospinning, Appl Biochem Biotechnol 190 (3) (2020) 1106-1123.
[34] W. Jia, P.S. Gungor-Ozkerim, Y.S. Zhang, K. Yue, K. Zhu, W. Liu, Q. Pi, B. Byambaa, M.R. Dokmeci, S.R. Shin, A. Khademhosseini, Direct 3D bioprinting of perfusable vascular constructs using a blend bioink, Biomaterials 106 (2016) 58-68.
[35] P. Datta, B. Ayan, I.T. Ozbolat, Bioprinting for vascular and vascularized tissue biofabrication, Acta Biomater 51 (2017) 1-20.
[36] S. Freeman, R. Ramos, P. Alexis Chando, L. Zhou, K. Reeser, S. Jin, P. Soman, K. Ye, A bioink blend for rotary 3D bioprinting tissue engineered small-diameter vascular constructs, Acta Biomater 95 (2019) 152-164.
[37] E. Akbari, G.B. Spychalski, K.K. Rangharajan, S. Prakash, J.W. Song, Flow dynamics control endothelial permeability in a microfluidic vessel bifurcation model, Lab Chip 18 (7) (2018) 1084-1093.
[38] X.Y. Wang, Y. Pei, M. Xie, Z.H. Jin, Y.S. Xiao, Y. Wang, L.N. Zhang, Y. Li, W.H. Huang, An artificial blood vessel implanted three-dimensional microsystem for modeling transvascular migration of tumor cells, Lab Chip 15 (4) (2015) 1178-1187.
[39] W.J. Polacheck, M.L. Kutys, J.B. Tefft, C.S. Chen, Microfabricated blood vessels for modeling the vascular transport barrier, Nat Protoc 14 (5) (2019) 1425-1454.
[40] K. Haase, R.D. Kamm, Advances in on-chip vascularization, Regen Med 12 (3) (2017) 285-302.
[41] A. Sobrino, D.T. Phan, R. Datta, X. Wang, S.J. Hachey, M. Romero-Lopez, E. Gratton, A.P. Lee, S.C. George, C.C. Hughes, 3D microtumors in vitro supported by perfused vascular networks, Sci Rep 6 (2016) 31589.
[42] H.Y. Mi, Y. Jiang, X. Jing, E. Enriquez, H. Li, Q. Li, L.S. Turng, Fabrication of triple-layered vascular grafts composed of silk fibers, polyacrylamide hydrogel, and polyurethane nanofibers with biomimetic mechanical properties, Mater Sci Eng C Mater Biol Appl 98 (2019) 241-249.
[43] R. Dong, Y. Liu, L. Mou, J. Deng, X. Jiang, Microfluidics-based biomaterials and biodevices, Adv Mater 31 (45) (2019) e1805033.
[44] P. Zhu, R. Chen, C. Zhou, M. Aizenberg, J. Aizenberg, L. Wang, Bioinspired soft microactuators, Adv Mater (2021) e2008558.
[45] X.Y. Du, Q. Li, G. Wu, S. Chen, Multifunctional micro/nanoscale fibers based on microfluidic spinning technology, Adv Mater 31 (52) (2019) e1903733.
[46] M.A. Daniele, D.A. Boyd, A.A. Adams, F.S. Ligler, Microfluidic strategies for design and assembly of microfibers and nanofibers with tissue engineering and regenerative medicine applications, Adv Healthc Mater 4 (1) (2015) 11-28.
[47] Y. Jun, E. Kang, S. Chae, S.H. Lee, Microfluidic spinning of micro- and nano-scale fibers for tissue engineering, Lab Chip 14 (13) (2014) 2145-2160.
[48] S. Shrestha, A. Kishen, Bioactive molecule delivery systems for dentin-pulp tissue engineering, J Endod 43 (5) (2017) 733-744.
[49] B.K. Gu, D.J. Choi, S.J. Park, Y.J. Kim, C.H. Kim, 3D bioprinting technologies for tissue engineering applications, Adv Exp Med Biol 1078 (2018) 15-28.

[50] H.W. Kang, S.J. Lee, I.K. Ko, C. Kengla, J.J. Yoo, A. Atala, A 3D bioprinting system to produce human-scale tissue constructs with structural integrity, Nat Biotechnol 34 (3) (2016) 312-319.
[51] G. Wang, L. Jia, F. Han, J. Wang, L. Yu, Y. Yu, G. Turnbull, M. Guo, W. Shu, B. Li, Microfluidics-based fabrication of cell-laden hydrogel microfibers for potential applications in tissue engineering, Molecules 24 (8) (2019) 1633.
[52] D.P. Lennon, A.I. Caplan, Isolation of rat marrow-derived mesenchymal stem cells, Exp Hematol 34(11) (2006) 1606-7.
[53] Y. Cao, S. Yang, D. Zhao, Y. Li, S.S. Cheong, D. Han, Q. Li, Three-dimensional printed multiphasic scaffolds with stratified cell-laden gelatin methacrylate hydrogels for biomimetic tendon-to-bone interface engineering, J Orthop Translat 23 (2020) 89-100.
[54] W. Shu, L. Liu, G. Bao, H. Kang, Tissue engineering of the temporomandibular joint disc: current status and future trends, Int J Artif Organs 38 (2) (2015) 55-68.
[55] D.F. Williams, Challenges with the development of biomaterials for sustainable tissue engineering, Front Bioeng Biotechnol 7 (2019) 127.
[56] P. Wu, Y. Liang, G. Sun, Engineering immune-responsive biomaterials for skin regeneration, Biomater Transl 2 (1) (2021) 61-71.
[57] Y. Gu, J. Zhang, X. Zhang, G. Liang, T. Xu, W. Niu, Three-dimensional printed Mg-doped beta-TCP bone tissue engineering scaffolds: effects of magnesium ion concentration on osteogenesis and angiogenesis in vitro, Tissue Eng Regen Med 16 (4) (2019) 415-429.
[58] L.J. Chen, H. Kaji, Modeling angiogenesis with micro- and nanotechnology, Lab Chip 17 (24) (2017) 4186-4219.
[59] L. Jia, F. Han, H. Yang, G. Turnbull, J. Wang, J. Clarke, W. Shu, M. Guo, B. Li, Microfluidic fabrication of biomimetic helical hydrogel microfibers for blood-vessel-on-a-chip applications, Adv Healthc Mater 8 (13) (2019) e1900435.
[60] X. Zhou, M. Nowicki, H. Sun, S.Y. Hann, H. Cui, T. Esworthy, J.D. Lee, M. Plesniak, L.G. Zhang, 3D bioprinting-tunable small-diameter blood vessels with biomimetic biphasic cell layers, ACS Appl Mater Interfaces 12 (41) (2020) 45904-45915.
[61] C. Grasl, M. Stoiber, M. Rohrich, F. Moscato, H. Bergmeister, H. Schima, Electrospinning of small diameter vascular grafts with preferential fiber directions and comparison of their mechanical behavior with native rat aortas, Mater Sci Eng C Mater Biol Appl 124 (2021) 112085.
[62] L. Bao, F.F. Hong, G. Li, G. Hu, L. Chen, Implantation of air-dried bacterial nanocellulose conduits in a small-caliber vascular prosthesis rabbit model, Mater Sci Eng C Mater Biol Appl 122 (2021) 111922.
[63] C. Hu, Y. Chen, M.J.A. Tan, K. Ren, H. Wu, Microfluidic technologies for vasculature biomimicry, Analyst 144 (15) (2019) 4461-4471.
[64] Y. Guo, J. Yan, J.H. Xin, L. Wang, X. Yu, L. Fan, P. Liu, H. Yu, Microfluidic-directed biomimetic Bulbine torta-like microfibers based on inhomogeneous viscosity rope-coil effect, Lab Chip (2021) 2594-2604.
[65] M. Khanmohammadi, S. Sakai, M. Taya, Fabrication of single and bundled filament-like tissues using biodegradable hyaluronic acid-based hollow hydrogel fibers, Int J Biol Macromol 104 (Pt A) (2017) 204-212.
[66] J. Yuan, P. Maturavogsadit, Z. Zhou, B. Lv, Y. Lin, J. Yang, J.A. Luckanagul, Hyaluronic acid-based hydrogels with tobacco mosaic virus containing cell adhesive peptide induce bone repair

in normal and osteoporotic rats, Biomater Transl, 1 (1) (2020) 89-98.
[67] L. Li, F. Yu, L. Zheng, R. Wang, W. Yan, Z. Wang, J. Xu, J. Wu, D. Shi, L. Zhu, X. Wang, Q. Jiang, Natural hydrogels for cartilage regeneration: Modification, preparation and application, J Orthop Translat 17 (2019) 26-41.
[68] G. Bahcecioglu, N. Hasirci, V. Hasirci, Cell behavior on the alginate-coated PLLA/PLGA scaffolds, Int J Biol Macromol 124 (2019) 444-450.
[69] P. Rastogi, B. Kandasubramanian, Review of alginate-based hydrogel bioprinting for application in tissue engineering, Biofabrication 11 (4) (2019) 042001.
[70] G. Zhang, Z. Wang, F. Han, G. Jin, L. Xu, H. Xu, H. Su, H. Wang, Y. Le, Y. Fu, J. Ju, L. Bin, R. Hou, Mechano-regulation of vascular network formation without branches in 3D bioprinted cell-laden hydrogel constructs, Biotechnol Bioeng (2021). DOI: 10.1002/bit.27854.
[71] D. Govindarajan, S. Nandhagopal, S. Shanmuganathan, J. Ramasamy, M.S. Kiran, Modular mucopolysaccharide gelatin naturapolyceutics hydrocolloid biomatrix with cobalt nano-additives for high density vascular network assembly, Int J Biol Macromol 181 (2021) 847-857.
[72] B.F.L. Lai, R.X.Z. Lu, L. Davenport Huyer, S. Kakinoki, J. Yazbeck, E.Y. Wang, Q. Wu, B. Zhang, M. Radisic, A well plate-based multiplexed platform for incorporation of organoids into an organ-on-a-chip system with a perfusable vasculature, Nat Protoc 16 (4) (2021) 2158-2189.
[73] C. Sturtzel, Endothelial cells, Adv Exp Med Biol 1003 (2017) 71-91.
[74] F. Jiang, Autophagy in vascular endothelial cells, Clin Exp Pharmacol Physiol 43 (11) (2016) 1021-1028.
[75] B.W. Wong, E. Marsch, L. Treps, M. Baes, P. Carmeliet, Endothelial cell metabolism in health and disease: impact of hypoxia, EMBO J 36 (15) (2017) 2187-2203.
[76] M. Moffa, A.G. Sciancalepore, L.G. Passione, D. Pisignano, Combined nano- and micro-scale topographic cues for engineered vascular constructs by electrospinning and imprinted micro-patterns, Small 10 (12) (2014) 2439-2450.